catalysts

MDPI

Article

Activated Carbon/MnO_2 Composites as Electrode for High Performance Supercapacitors

Jang Rak Choi [1,2], Ji Won Lee [1], Guijun Yang [1], Young-Jung Heo [1] and Soo-Jin Park [1,*]

[1] Department of Chemistry, Inha University, 100 Inharo, Incheon 22212, Korea; 22161120@inha.edu (J.R.C.); lj529@naver.com (J.W.L.); yanggj@inha.edu (G.Y.); heoyj1211@inhaian.net (Y.-J.H.)

[2] Evertech Enterprise Co. Ltd., Dongtansandan 2 gil, Hwaseong 18487, Korea

* Correspondence: sjpark@inha.ac.kr; Tel.: +82-32-876-7234

Received: 13 January 2020; Accepted: 19 February 2020; Published: 20 February 2020

Abstract: Activated carbon (AC) was synthesized with various weight ratios of manganese dioxide (MO) through a simple hydrothermal approach. The electrochemical performance of the synthesized activated carbon/MnO_2 composites was investigated. The effect of the activated carbon/MnO_2 (AM) ratio on the electrochemical properties of the activated carbon/MnO_2 composites and the pore structure was also examined. The results show that the specific capacitance of the activated carbon material has been improved after the addition of MO. The as-synthesized composite material exhibits specific capacitance of 60.3 F g^{-1} at 1 A g^{-1}, as well as stable cycle performance and 99.6% capacitance retention over 5000 cycles.

Keywords: activated carbon; manganese dioxide; electrochemical performance; supercapacitor

1. Introduction

With global warming and a worsening environment, the use of renewable energy sources is becoming increasingly important [1,2]. In order to use renewable energy effectively, flexible and scalable energy storage solutions must be adopted for energy storage [3,4]. Electrochemical energy storage (EES) devices are particularly suitable for portable electronic equipment or hybrid electric vehicles. Among different kind of EES devices, supercapacitors (SCs) have the characteristics of a long cycling life and high power density, and have broad application prospects in many fields [5]. Generally, SCs can be classified into two types: electric double layer capacitors (EDLCs) and pseudocapacitors [6,7]. The capacitance of EDLCs mainly depends on the adsorption of anions and cations on or near the electrode/electrolyte interface, which is mainly related to the surface area of the electrode material. Porous carbon, such as in activated carbon [8,9], carbon nanotubes [10,11], carbon nanofibers [12,13] and graphene [14,15], is a commonly used electrode material for EDLCs. This kind of carbon material has a high specific surface area and good conductivity, which can improve higher specific capacitance. Although graphene and carbon nanotubes have better conductivity and surface area than other carbons, activated carbon has become an ideal electrode material for EDLCs, and is used on a large scale for commercialized supercapacitors due to its easy processing and lower cost, adjustable surface area, relatively inert electrochemical properties, adjustable porosity and electrocatalytically active sites for reactions. However, the energy density of carbon-based materials is relatively low, and the volume energy density particularly needs to be further improved [16–18].

Generally, there are two main solutions to improve the performance of AC material. First, the physical or chemical activation of activated carbon can be used to control pore characteristics and increase surface area, thereby increasing the specific capacitance [19]. Physical activation leads to a more concentrated pore size distribution, while chemical activation can increase the bulk density and thus increase the adsorption capacity [20,21]. The second is to combine the carbon material with metal

oxide or a conductive polymer to enhance the capacitance performance through the synergy effect of EDLC and the pseudocapacitors [22]. For instance, Cao et al. [23] synthesized NiO/activated carbon composites and obtained a specific capacitance of 214.48 F g^{-1} at 40 mA g^{-1} in a 1 M KOH aqueous solution. Kim et al. [24] prepared activated carbon nanotube/CuO composites to obtain enhanced specific capacitance. In addition, 2D metal carbides and nitrides (MXenes) are also a very promising supercapacitor material. Due to the surface termination of MXenes being able to be adjusted, as well as incorporated into activated carbon/MnO_2 materials, there are many reports using MXenes to enhance specific capacitance [25–27]. The specific capacitance of the prepared composite electrode combines a double layer of capacitance and pseudocapacitance; this kind of combination greatly improves the electrochemical performance of composite materials.

Herein, we prepared activated carbon/manganese dioxide (AC/MO) composites with various weight ratios of manganese dioxide (MO). The electrochemical performance of the synthesized composites with different weight ratios of MO was investigated. Furthermore, the influence of MO content on the pore characteristics of AC was also studied. The as-synthesized AC/MO composites showed more enhanced electrochemical performance than both the pure MO and AC, and it is a promising alternative carbon material for the application of SCs.

2. Results and Discussion

2.1. Structural Properties

The chemical states data of the AM composites were collected by XPS. The XPS spectrum of Figure 1a indicates the existence of Mn, O and C, and the peak intensity of Mn2p and O1s increases with the increase of MO content (Table 1). When spin energy was used to separate 11.6 eV, characteristic peaks of $Mn2p_{1/2}$ (653.8 eV) and $Mn2p_{3/2}$ (642.2 eV) appeared, indicating that MO was successfully coated on the AM1 composites [28,29]. The O1s XPS spectrum of AC, AM1 is shown in Figure 1c. The characteristic peaks at 531.9 eV and 534.8 eV belong to the characteristic peaks of C=O (531.9 eV) of AC and H_2O (534.8 eV), respectively. In addition, there are three peaks concentrated at 529.9, 531.4 and 533.4 eV, which corresponds to the Mn–O–Mn bond, Mn–O–H bond and H–O–H bond of MO [30,31].

The morphology and structure of AC, AM1 composites can be further investigated by SEM. AC has a smooth surface and a size of approximately 10–170 μm in shape, shown as irregular pieces in Figure 2a. In addition, Figure 2b also has an irregular shape; a magnified SEM image of the sample in Figure 2b indicates MnO_2 as a sphere nanostructure particle. The cross-sectional SEM and energy dispersive X-ray spectroscopy (EDS) mapping images of the AM0.1, AM1 and AM3 composites are shown in Figure 2c. The EDS mapping images of the composites is also shown in Figure 2c, which indicates that the samples consisted of C and Mn. The Mn peaks of AM1 and AM3 were more distinct than that of AM0.1. The Mn content in the AC material increases with the addition of MO [32,33].

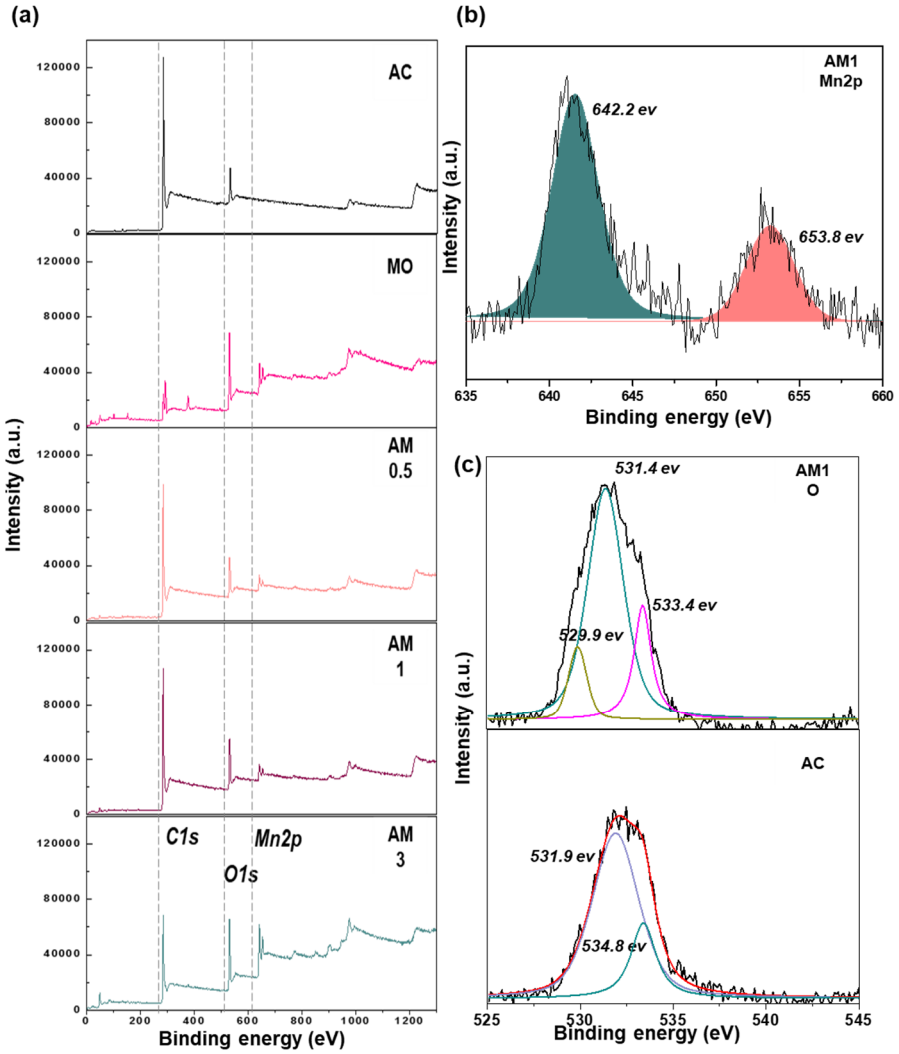

Figure 1. X-ray photoelectron spectroscopy spectra of AC, MO and AM composites: (**a**) survey scan; (**b**) Mn2p spectrum; and (**c**) O spectrum of AM1 composites.

Table 1. Elemental properties of the as-synthesized samples.

Sample	X-ray Photoelectron Spectroscopy (at. %)			ICP-OES (at. %)
	C	O	Mn	Mn
AC	81.34	18.66	-	-
MO	-	74.85	25.10	28.61
AM 0.1	85.34	13.45	1.15	2.17
AM 0.5	82.45	15.26	3.00	4.69
AM 1	71.73	24.53	3.75	7.96
AM 2	71.19	23.40	5.41	9.13
AM 3	63.22	28.85	7.93	12.37

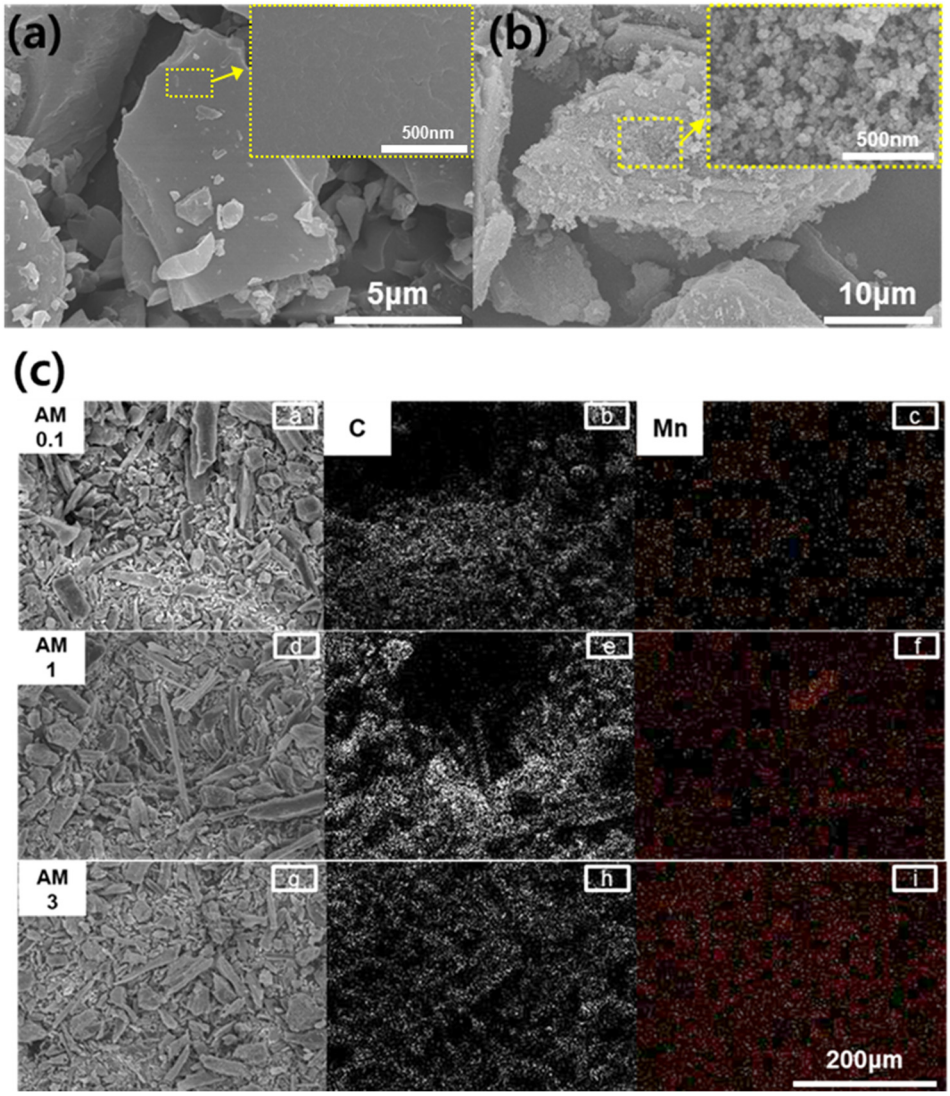

Figure 2. Scanning electron microscopy (SEM) images for (**a**) AC; (**b**) AM1 composites; and (**c**) Scanning electron microscopy with energy dispersive X-ray spectroscopy (SEM-EDS) mapping of AM0.1, AM1, and AM3 composites: (c-a, c-d and c-g) SEM images, (c-b, c-e and c-h) C distribution and (c-e, c-f and c-i) Mn distribution.

The surface and pore information of the prepared composites were measured by the nitrogen adsorption-desorption method. The specific surface areas of AC, MO and AM composites were calculated by utilizing the BET equation. Figure 3a shows the nitrogen adsorption/desorption isotherms of AC, MO and AM composites at 77 K. All samples showed typical IUPAC type isotherms [34]. The results at the relative pressure of $P{\cdot}P_0{}^{-1}$ = 0.1 provide proof of the existence of variously sized microporous structures. Figure 3b shows the pore size distribution of the samples, indicating that the pores in the samples were micropores (<2 nm) and mesopores (<50 nm) [35]. The porous information of the as-prepared samples, which is calculated from BET, is summarized in Table 2. The specific surface area of pure AC was 1844 m^2 g^{-1}, while the BET surface areas of AM0.1, AM0.5, AM1, AM2 and AM3 were calculated to be 1505, 1569, 1479, 1172 and 1017 m^2 g^{-1}, respectively. The total volumes of AM0.1, AM0.5, AM1, AM2 and AM3 were calculated to be 1.047, 1.099, 1.047, 0.817 and 0.708 cm^3 g^{-1}, respectively. In summary, since the injected MO blocked the pore structure, the specific surface area and micropore volume of the composites decreased with the increase of MO content.

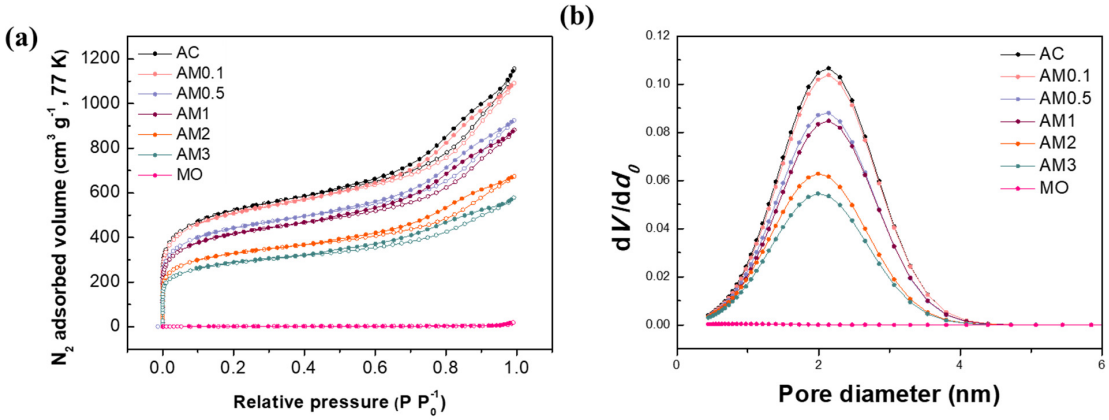

Figure 3. (**a**) N_2 adsorption/desorption isotherms (solid symbols represent desorption isotherms, and hollow symbols represent adsorption isotherms); and (**b**) pore size distributions of AC, MO and the AM composites.

Table 2. The porous parameter of the as-synthesized samples.

Samples	[a] S_{BET} (m^2 g^{-1})	[b] V_{total} (cm^3 g^{-1})	[c] V_{meso} (cm^3 g^{-1})	[d] V_{micro} (cm^3 g^{-1})	[e] D_p (nm)
AC	1844	1.316	0.526	0.790	3.8
AM 0.1	1805	1.047	0.419	0.628	3.7
AM 0.5	1569	1.099	0.427	0.672	3.6
AM 1	1479	1.047	0.419	0.628	3.6
AM 2	1172	0.817	0.276	0.541	3.5
AM 3	1017	0.708	0.239	0.469	3.4
MO	4	0.002	0.002	0.000	28.1

2.2. *Electrochemical Performance of AM Composites*

The electrochemical properties of AC, MO and AM composites for electrochemical capacitor application are calculated and shown in Figure 4. Figure 4a shows the galvanostatic charge-discharge (GCD) curves of AC, MO and AM composites at 1 A g^{-1}. The specific capacitance of the as-prepared electrodes was calculated according to Equation (1)

$$C_m = \frac{I \times t}{\Delta V \times m} \quad (1)$$

where C_m is the specific capacitance [F g^{-1}], I is the charge/discharge current, t is the charge/discharge time, ΔV is the potential window and m is the mass of active material [36,37]. The highest obtained specific capacitance, obtained with AM1, was 60.3 F g^{-1} at 1 A g^{-1}. The high specific capacitance results in the proper combination of AC and MO components. The comparison of the specific capacitance of this work with that of other literature was shown in Table 3.

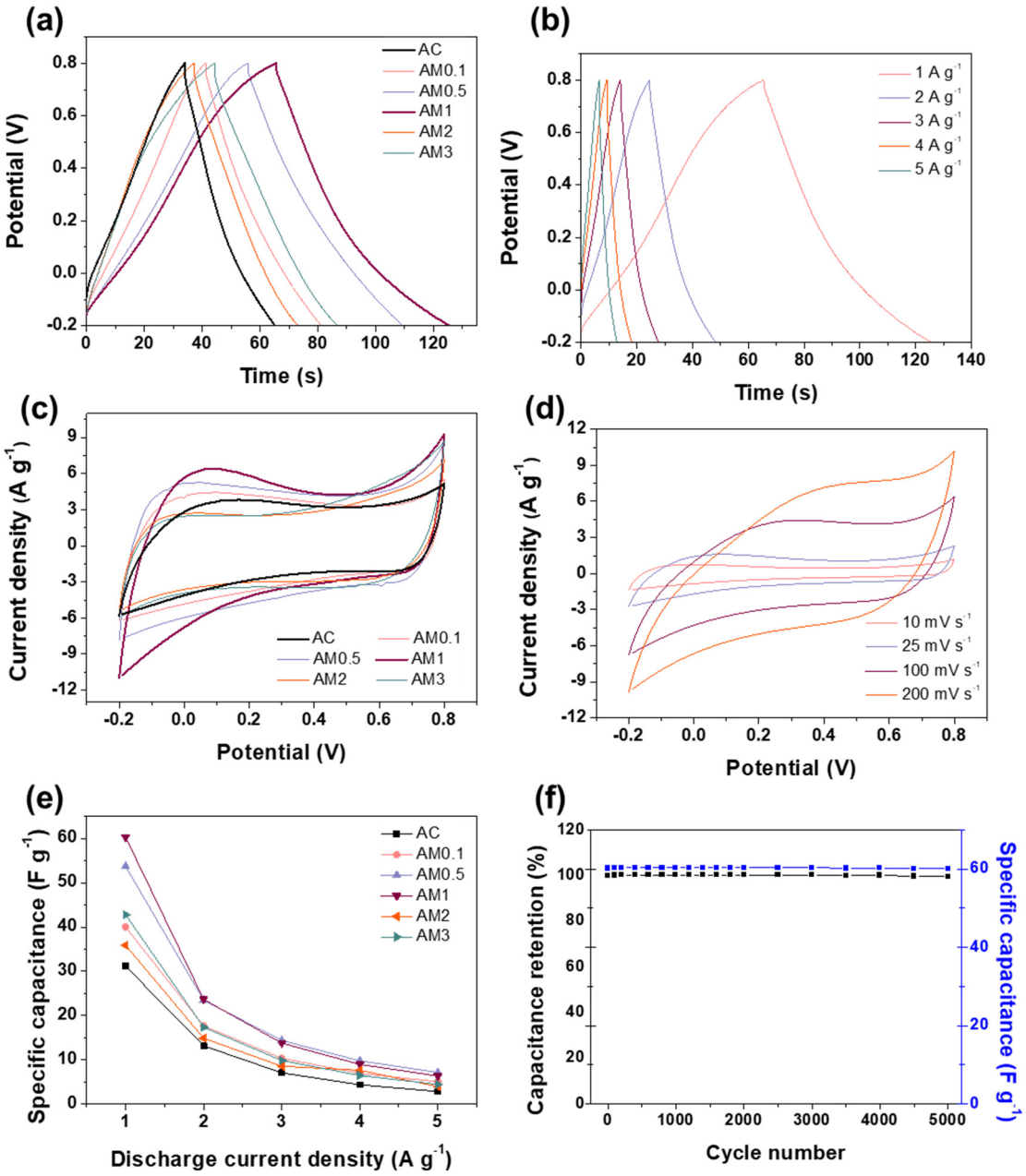

Figure 4. (**a**) Galvanostatic charge/discharge curves of the prepared composites at 1 A g^{-1}; (**b**) galvanostatic charge/discharge curves of the AM1 composite electrodes at different current densities (1–5 A g^{-1}); (**c**) cyclic voltammograms of the prepared samples at a scan rate of 100 mV s^{-1}; (**d**) cyclic voltammograms of the AM1 composite electrodes at different scan rates; (**e**) comparison of the specific capacitances of AC, MO and AM composites; and (**f**) cycling performance of AM1 composite electrodes at 100 mV s^{-1} for 5000 cycles.

Table 3. Comparison of the specific capacitance of this work with that of other literature.

Sample	Specific Capacitance (F g^{-1})	Ref.
MnO_2/Activated carbon	62.4 (0.1 A g^{-1})	[38]
$LiMn_2O_4$/Activated carbon	48 (1 A g^{-1})	[39]
$ZnCl_2$ treated activated carbon	74 (0.5 A g^{-1})	[40]
Activated carbon/MnO_2	60.3 (1 A g^{-1})	This work

Figure 4b indicates the GCD curves of the AM1 electrode at various current densities (1, 2, 3, 4 and 5 A g^{-1}). The specific capacitance of the AM1 electrode decreases with the increase of the discharge current density. This is mainly because the electrolyte ions diffuse slowly at high current densities, and cannot penetrate the active material sufficiently [41]. Figure 4c shows the CV curves of the as-prepared composites electrodes at 100 mV s^{-1}. The CV curve of AC presents a relatively regular rectangle, and the potential of each terminal does not show a rapid current response to the potential inversion, indicating that the AC material has largely maintained the characteristics of EDLCs. Moreover, the rectangular area of the CV curve of the AM composite was greatly improved by the redox transition of MO between the semiconductor state and the conduction state, thereby improving the redox capacitance. The area of the CV curve increased from AM0.1 to AM1, but with the higher MO concentrations in AM2 and AM3, this area gradually decreased. The AM1 electrode gave rise to the largest CV curve area among the examined electrodes, as AM1 has good conductivity and can provide an electron transfer path. Therefore, compared with other sample electrodes, the AM1 electrode has lower resistance and more ideal supercapacitor characteristics.

To investigate the EDLC behavior of the AM1 composite electrode in more detail, the CV curves at various scan rates (10, 25, 100 and 200 mV s^{-1}) were tested. Figure 4d indicates that the CV curve of AM1 shows an approximately symmetrical rectangle shape. This shows that AM1 has good pseudocapacitive and EDLC behavior. Figure 4e summarizes the specific capacitance of the AC and AM composite electrodes at various current densities. The AM composite electrode shows an enhanced area capacitance with increasing MO content, with the increase of the scan rate ranging from 1 to 5 mV s^{-1}. The capacitance of the AM1 electrode was 60.3 F g^{-1} at a current density of 1 A g^{-1}, which was higher than that of AC and the other AM composites. The retained capacitances of the AC, AM0.1, AM0.5, AM1, AM2 and AM3 composite electrodes were 9.29%, 12.75%, 13.4%, 10.6%, 11.1% and 10.5% from 1 to 5 A g^{-1}, attributed to the relatively slow faradic reactions. Furthermore, the cycling performance of the AM1 was investigated at 100 mV s^{-1} (Figure 4f). AM1 exhibited a stable cycling performance, and maintained a 99.6% capacity retention rate after 5000 cycles. Notably, the CV curves were still symmetric after 5000 cycles, indicating no significant structural changes of the AM1 electrode during the CV processes.

3. Chemicals and Synthesis

3.1. Chemicals and Composites Synthesis

Activated carbon (AC; LG Co. Seoul, South Korea), manganese dioxide (MnO_2, ≥90%, Sigma–Aldrich Co. Seoul, South Korea), 0.5 g of AC and 0.1 g of MO (AC:MO (mass ratio) = 5:0.1, 5:0.5, 5:1, 5:2 and 5:3) were distributed uniformly in 50 mL of deionized water at 25 °C. Secondly, the mixture was transferred to a Teflon stainless-steel autoclave and reacted at 120 °C for 4 h. Finally, the as-synthesized AM precursor was washed with deionized water several times, and then dried overnight under a vacuum at 80 °C. The as-synthesized AM was then annealed at 400 °C for 1 h under N_2 atmosphere. The as-prepared composites are denoted as AM0.1, AM0.5, AM1, AM2 and AM3, according to the manganese dioxide content.

3.2. Structural Characterizations

X-ray photoelectron spectroscopy (XPS, Thermo Scientific, Waltham, MA, United States) data were used to test the surface chemical composition of the sample. Scanning electron microscopy (SEM, Model SU8010, Hitachi Co., Ltd., Tokyo, Japan) with energy dispersive X-ray spectroscopy (EDS) mapping was used to analyze the prepared composites. N_2 adsorption/desorption isotherms were collected by a gas adsorption analyzer (BEL, BELSORP-max, Tokyo, Japan). The element composition of the composites was determined by inductively coupled plasma-optical emission spectrometry (ICP-OES, Piscataway, NJ, United States).

3.3. Electrode Preparation and Electrochemical Measurements

The active material, carbon black and polyvinylidene difluoride (PVDF) are mixed in a weight ratio of 8:1:1 to prepare a working electrode slurry, with NMP acting as the solvent. The prepared working electrode slurry is evenly coated on nickel foam through the drop-casting method, and dried at 60 °C for 12 h. The as-prepared AC and AM composite electrodes were studied in Na_2SO_4 electrolyte (1 mol L^{-1}). The three-electrode system was assembled with a platinum wire as the counter electrode, and an Ag/AgCl electrode as the reference electrode to test the electrochemical performance of the as-prepared materials. CV curves were obtained at various scan rates (10, 25, 100 and 200 mV s^{-1}) at a potential window of −0.2–0.8 V. GCD curves were tested at various current densities from 1 to 5 A g^{-1} within the same potential window.

4. Conclusions

In summary, AM composites with various mass ratios of MO were synthesized by the facile hydrothermal method. The AM composite electrodes exhibited higher specific capacitance than pure AC or MO electrodes. The effect of MnO_2 on the electrochemical performance was evaluated by varying the AC:MO ratio. In a certain range, the addition of MnO_2 improved the electrochemical performance of activated carbon, but with the increase of MnO_2 addition, the excess porosity of MnO_2 will cause a decrease of porosity, which will cause a decrease of the electrochemical performance of AM composites. The optimal ratio of AM composite is an AC:MO ratio of 1:1 (weight ratio). The electrochemical performance data indicated that the AM composites exhibit a good specific capacitance (60.3 F g^{-1}) and rate performance. Furthermore, the AM composite electrodes exhibited significantly improved cycling stability.

Author Contributions: Conceptualization and supervision, J.R.C., J.W.L., G.Y., Y.-J.H. investigation, writing-original draft preparation; S.-J.P. supervision, project administration and funding acquisition. All authors have read and agreed to the published version of the manuscript.

Funding: This research was supported by the Technology Innovation Program (or Industrial Strategic Technology Development Program) (10080293, Development of carbon-based non-phenolic electrode materials with 3000 m^2 g^{-1} grade surface area for energy storage device) and the Technological Innovation R&D Program (S2829590) funded by the Small and Medium Business Administration (SMBA, Korea).

Conflicts of Interest: The authors declare no conflict of interest.

References

1. Sun, Y.; Sills, R.B.; Hu, X.; Seh, Z.W.; Xiao, X.; Xu, H.; Luo, W.; Jin, H.; Xin, Y.; Li, T. A bamboo-inspired nanostructure design for flexible, foldable, and twistable energy storage devices. *Nano Lett.* **2015**, *15*, 3899–3906. [CrossRef]
2. Seh, Z.W.; Kibsgaard, J.; Dickens, C.F.; Chorkendorff, I.; Nørskov, J.K.; Jaramillo, T.F. Combining theory and experiment in electrocatalysis: Insights into materials design. *Science* **2017**, *355*, eaad4998. [CrossRef] [PubMed]
3. Ghidiu, M.; Lukatskaya, M.R.; Zhao, M.-Q.; Gogotsi, Y.; Barsoum, M.W. Conductive two-dimensional titanium carbide 'clay'with high volumetric capacitance. *Nature* **2014**, *516*, 78. [CrossRef] [PubMed]
4. Janoschka, T.; Martin, N.; Martin, U.; Friebe, C.; Morgenstern, S.; Hiller, H.; Hager, M.D.; Schubert, U.S. An aqueous, polymer-based redox-flow battery using non-corrosive, safe, and low-cost materials. *Nature* **2015**, *527*, 78. [CrossRef] [PubMed]
5. Miller, J.R.; Simon, P. Electrochemical capacitors for energy management. *Science* **2008**, *321*, 651–652. [CrossRef]
6. Lee, Y.J.; Park, H.W.; Park, S.; Song, I.K. Electrochemical properties of Mn-doped activated carbon aerogel as electrode material for supercapacitor. *Curr. Appl. Phys.* **2012**, *12*, 233–237. [CrossRef]
7. Yang, G.; Park, S.-J. Facile hydrothermal synthesis of NiCo2O4-decorated filter carbon as electrodes for high performance asymmetric supercapacitors. *Electrochim. Acta* **2018**, *285*, 405–414. [CrossRef]

8. Yaglikci, S.; Gokce, Y.; Yagmur, E.; Aktas, Z. The performance of sulphur doped activated carbon supercapacitors prepared from waste tea. *Environ. Technol.* **2020**, *41*, 36–48. [CrossRef]
9. Huang, Y.; Shi, Y.; Gong, Q.; Weng, M.; Li, Y.; Gan, J.; Wang, D.; Shao, Y.; Zhao, M.; Zhuang, D. Scalable preparation of hierarchical porous activated carbon/graphene composites for high-performance supercapacitors. *J. Mater. Chem. A* **2019**, *7*, 10058–10066. [CrossRef]
10. Zhang, Z.; Wang, L.; Li, Y.; Wang, Y.; Zhang, J.; Guan, G.; Pan, Z.; Zheng, G.; Peng, H. Nitrogen-Doped Core-Sheath Carbon Nanotube Array for Highly Stretchable Supercapacitor. *Adv. Energy Mater.* **2017**, *7*, 1601814. [CrossRef]
11. Liu, J.-h.; Xu, X.-y.; Yu, J.; Hong, J.-l.; Liu, C.; Ouyang, X.; Lei, S.; Meng, X.; Tang, J.-N.; Chen, D.-Z. Facile construction of 3D porous carbon nanotubes/polypyrrole and reduced graphene oxide on carbon nanotube fiber for high-performance asymmetric supercapacitors. *Electrochim. Acta* **2019**, *314*, 9–19. [CrossRef]
12. Chang, W.-M.; Wang, C.-C.; Chen, C.-Y. Fabrication of ultra-thin carbon nanofibers by centrifuged-electrospinning for application in high-rate supercapacitors. *Electrochim. Acta* **2019**, *296*, 268–275. [CrossRef]
13. Yang, G.; Park, M.; Park, S.-J. Recent progresses of fabrication and characterization of fibers-reinforced composites: A review. *Compos. Commun.* **2019**, *14*, 34–42. [CrossRef]
14. Ke, Q.; Wang, J. Graphene-based materials for supercapacitor electrodes—A review. *J. Mater.* **2016**, *2*, 37–54. [CrossRef]
15. Li, H.; Tao, Y.; Zheng, X.; Luo, J.; Kang, F.; Cheng, H.-M.; Yang, Q.-H. Ultra-thick graphene bulk supercapacitor electrodes for compact energy storage. *Energy Environ. Sci.* **2016**, *9*, 3135–3142. [CrossRef]
16. Misnon, I.I.; Zain, N.K.M.; Jose, R. Conversion of oil palm kernel shell biomass to activated carbon for supercapacitor electrode application. *Waste Biomass Valorization* **2019**, *10*, 1731–1740. [CrossRef]
17. Prataap, R.V.; Arunachalam, R.; Raj, R.P.; Mohan, S.; Peter, L. Effect of electrodeposition modes on ruthenium oxide electrodes for supercapacitors. *Curr. Appl. Phys.* **2018**, *18*, 1143–1148. [CrossRef]
18. Ensafi, A.A.; Alinajafi, H.A.; Rezaei, B. Adenine decorated@ reduced graphene oxide, a new environmental friendly material for supercapacitor application. *J. Alloy. Compd.* **2018**, *735*, 1010–1016. [CrossRef]
19. Yumak, T. Electrochemical Performance of Fabricated Supercapacitors Using MnO2/Activated Carbon Electrodes. *Hacet. J. Biol. Chem.* **2019**, *47*, 115–122.
20. Williams, P.T.; Reed, A.R. Development of activated carbon pore structure via physical and chemical activation of biomass fibre waste. *Biomass Bioenergy* **2006**, *30*, 144–152. [CrossRef]
21. Prauchner, M.J.; Rodríguez-Reinoso, F. Chemical versus physical activation of coconut shell: A comparative study. *Microporous Mesoporous Mater.* **2012**, *152*, 163–171. [CrossRef]
22. Ho, M.; Khiew, P.; Isa, D.; Tan, T.; Chiu, W.; Chia, C.H. A review of metal oxide composite electrode materials for electrochemical capacitors. *Nano* **2014**, *9*, 1430002. [CrossRef]
23. Cao, J.-P.; He, S.; Wu, Y.; Zhao, X.-Y.; Wei, X.-Y.; Takarada, T. Synthesis of NiO/Activated Carbon Composites and Their Application as Electrode Materials for Capacitors. *Int. J. Electrochem. Sci* **2017**, *12*, 2704–2718. [CrossRef]
24. Kim, D.-W.; Rhee, K.-Y.; Park, S.-J. Synthesis of activated carbon nanotube/copper oxide composites and their electrochemical performance. *J. Alloy. Compd.* **2012**, *530*, 6–10. [CrossRef]
25. Lukatskaya, M.R.; Dunn, B.; Gogotsi, Y. Multidimensional materials and device architectures for future hybrid energy storage. *Nat. Commun.* **2016**, *7*, 1–13. [CrossRef] [PubMed]
26. Anasori, B.; Lukatskaya, M.R.; Gogotsi, Y. 2D metal carbides and nitrides (MXenes) for energy storage. *Nat. Rev. Mater.* **2017**, *2*, 1–17. [CrossRef]
27. Zhang, C.; Kremer, M.P.; Seral-Ascaso, A.; Park, S.H.; McEvoy, N.; Anasori, B.; Gogotsi, Y.; Nicolosi, V. Stamping of flexible, coplanar micro-supercapacitors using MXene inks. *Adv. Funct. Mater.* **2018**, *28*, 1705506. [CrossRef]
28. Patil, A.; Lokhande, A.; Chodankar, N.; Kumbhar, V.; Lokhande, C. Engineered morphologies of β-NiS thin films via anionic exchange process and their supercapacitive performance. *Mater. Des.* **2016**, *97*, 407–416. [CrossRef]
29. Yang, G.; Park, S.-J. MnO2 and biomass-derived 3D porous carbon composites electrodes for high performance supercapacitor applications. *J. Alloy. Compd.* **2018**, *741*, 360–367. [CrossRef]

30. Tseng, L.-H.; Hsiao, C.-H.; Nguyen, D.D.; Hsieh, P.-Y.; Lee, C.-Y.; Tai, N.-H. Activated carbon sandwiched manganese dioxide/graphene ternary composites for supercapacitor electrodes. *Electrochim. Acta* **2018**, *266*, 284–292. [CrossRef]
31. Babkova, T.; Fei, H.; Kazantseva, N.E.; Sapurina, I.Y.; Sáha, P. Enhancing the supercapacitor performance of flexible MnOxCarbon cloth electrodes by Pd-decoration. *Electrochim. Acta* **2018**, *272*, 1–10. [CrossRef]
32. Han, G.; Liu, Y.; Zhang, L.; Kan, E.; Zhang, S.; Tang, J.; Tang, W. MnO 2 nanorods intercalating graphene oxide/polyaniline ternary composites for robust high-performance supercapacitors. *Sci. Rep.* **2014**, *4*, 4824. [CrossRef] [PubMed]
33. Sidheswaran, M.A.; Destaillats, H.; Sullivan, D.P.; Larsen, J.; Fisk, W.J. Quantitative room-temperature mineralization of airborne formaldehyde using manganese oxide catalysts. *Appl. Catal. B Environ.* **2011**, *107*, 34–41. [CrossRef]
34. Ali, G.A.; Yusoff, M.M.; Ng, Y.H.; Lim, H.N.; Chong, K.F. Potentiostatic and galvanostatic electrodeposition of manganese oxide for supercapacitor application: A comparison study. *Curr. Appl. Phys.* **2015**, *15*, 1143–1147. [CrossRef]
35. Lee, H.I.; Park, S.-J. One-pot synthesis of reduced graphene oxide/anatase titanium dioxide composites for photocatalytic degradation of methylene blue. *J. Nanosci. Nanotechnol.* **2018**, *18*, 6173–6179. [CrossRef] [PubMed]
36. Mishra, R.K.; Manivannan, S.; Kim, K.; Kwon, H.-I.; Jin, S.H. Petal-like MoS2 nanostructures with metallic 1 T phase for high performance supercapacitors. *Curr. Appl. Phys.* **2018**, *18*, 345–352. [CrossRef]
37. Yang, C.-S.; Jang, Y.S.; Jeong, H.K. Bamboo-based activated carbon for supercapacitor applications. *Curr. Appl. Phys.* **2014**, *14*, 1616–1620. [CrossRef]
38. Yuan, A.; Zhang, Q. A novel hybrid manganese dioxide/activated carbon supercapacitor using lithium hydroxide electrolyte. *Electrochem. Commun.* **2006**, *8*, 1173–1178. [CrossRef]
39. Malak-Polaczyk, A.; Matei-Ghimbeu, C.; Vix-Guterl, C.; Frackowiak, E. Carbon/λ-MnO2 composites for supercapacitor electrodes. *J. Solid State Chem.* **2010**, *183*, 969–974. [CrossRef]
40. Subramanian, V.; Luo, C.; Stephan, A.M.; Nahm, K.S.; Thomas, S.; Wei, B. Supercapacitors from Activated Carbon Derived from Banana Fibers. *J. Phys. Chem. C* **2007**, *111*, 7527–7531. [CrossRef]
41. Kim, T.-W.; Park, S.-J. Synthesis of reduced graphene oxide/thorn-like titanium dioxide nanofiber aerogels with enhanced electrochemical performance for supercapacitor. *J. Colloid Interface Sci.* **2017**, *486*, 287–295. [CrossRef] [PubMed]